DOI 10.15507/2079-6900.27.202504.500-516
Original article
ISSN 2079-6900 (Print)
ISSN 2587-7496 (Online)

MSC2020 65M06, 85-10

2D model of the hydrodynamic escape of planetary atmospheres

K. D. Gorbunova, N. V. Erkaev

Institute of Computational Modelling, Siberian Branch of Russian Academy of Science (Krasnoyarsk, Russian Federation)

Abstract. The article considers a two-dimensional problem of hydrodynamic escape of the planet's primordial hydrogen atmosphere as a result of absorption of extreme ultraviolet (EUV) radiation from its host star. As a test case, the model is applied using the parameters of a recently discovered exoplanet TOI-421b, which, according to accepted classification, belongs to so-called class of "warm mini-Neptunes". The hydrodynamic parameters are determined by solving the non-stationary Euler and entropy production equations in a spherical coordinate system. The EUV intensity is calculated using the radiation transport equation along parallel rays, with an absorption coefficient proportional to the density of the hydrogen atoms. The numerical method is based on a finite-difference scheme of the modified MacCormack — Runge–Kutta type on a spherical grid with a nonuniform step along the radial direction and a constant step along the spherical angle. The calculation of the radiation intensity at the grid points is perfomed along the characteristics with density interpolation. Steady-state two-dimensional profiles of physical parameters in the upper atmosphere obtained as the result of calculations are presented. An estimate of the dayside atmospheric mass-loss rate and the rate of mass transfer to the nightside under constant external conditions is provided.

Keywords: mathematical modelling, exoplanet, upper atmospheres, two-dimensional problem, atmospheric escape

For citation: *K. D. Gorbunova, N. V. Erkaev.* 2D model of the hydrodynamic escape of planetary atmospheres. *Zhurnal Srednevolzhskogo matematicheskogo obshchestva.* 27:4(2025), 500–516. DOI: 10.15507/2079-6900.27.202504.500-516

About the authors:

Kseniia D. Gorbunova, Engineer, Department of Computational Physics, Institute of Computational Modelling, Siberian Branch of Russian Academy of Science (50/44, Akademgorodok, Krasnoyarsk, 660036, Russian Federation), ORCID: http://orcid.org/0009-0000-7593-3874, gorbunova.kd@icm.krasn.ru

Nikolay V. Erkaev, Dr.Sci. (Phys. and Math.), Chief researcher, Institute of Computational Modelling, Siberian Branch of Russian Academy of Science (50/44, Akademgorodok, Krasnoyarsk, 660036, Russian Federation), ORCID: http://orcid.org/0000-0001-8993-6400, erkaev@icm.krasn.ru

© *K. D. Gorbunova, N. V. Erkaev*

Контент доступен по лицензии Creative Commons Attribution 4.0 International License.
This is an open access article distributed under the terms of the Creative Commons Attribution 4.0 International License.

Оригинальная статья

УДК 519.6 : 52.4

2D моделирование гидродинамического истечения планетарных атмосфер

К. Д. Горбунова, Н. В. Еркаев

Институт вычислительного моделирования Сибирского отделения Российской академии наук (г. Красноярск, Российская Федерация)

Аннотация. В статье рассматривается двумерная задача о гидродинамическом истечении первичной водородной атмосферы планеты в результате поглощения экстремального ультрафиолетового излучения (EUV) от родительской звезды. В качестве примера приведены параметры недавно открытой экзопланеты TOI-421b, которая, согласно принятой классификации, относится к так называемому классу "теплых мини-Нептунов". Гидродинамические параметры определяются путем решения нестационарных уравнений Эйлера и производства энтропии в сферической системе координат. Для определения интенсивности EUV применяется уравнение переноса излучения вдоль параллельных лучей с коэффициентом поглощения, пропорциональным плотности атомов водорода. Численный метод основан на конечно-разностной схеме модифицированного типа МакКормака — Рунге–Кутты на сферической сетке с неравномерным шагом по радиальному направлению и постоянным шагом по сферическому углу. Расчет интенсивности излучения в точках сетки выполняется по характеристикам с интерполяцией плотности. Представлены стационарные двумерные профили физических параметров в верхних слоях атмосферы, полученные в результате расчетов. Приводится оценка скорости истечения массы атмосферы на дневной стороне планеты и скорость ухода массы на ночную сторону планеты при постоянных внешних условиях.

Ключевые слова: математическое моделирование, экзопланеты, верхние атмосферы, двумерная задача, потеря массы атмосферы

Для цитирования: Горбунова К. Д., Еркаев Н. В. 2D моделирование гидродинамического истечения планетарных атмосфер // *Журнал Средневолжского математического общества.* 2025. Т. 27, № 4. С. 500-516. DOI: 10.15507/2079-6900.27.202504.500-516

Об авторах:

Горбунова Ксения Дмитриевна, инженер, Отдел вычислительной физики, Институт вычислительного моделирования Сибирского отделения Российской академии наук (660036, Россия, г. Красноярск, ул. Академгородок, д. 50/44), ORCID: http://orcid.org/0009-0000-7593-3874, gorbunova.kd@icm.krasn.ru

Еркаев Николай Васильевич, д.ф.-м.н., главный научный сотрудник, Отдел вычислительной физики, Институт вычислительного моделирования Сибирского отделения Российской академии наук (660036, Россия, г. Красноярск, ул. Академгородок, д. 50/44), ORCID: http://orcid.org/0000-0001-8993-6400, erkaev@icm.krasn.ru

1. Introduction

In recent years, atmospheric modeling has gained importance due to the discovery of numerous exoplanets and the study of their evolution. The loss of atmospheric particles under the action of external ultraviolet radiation is of crucial importance for understanding

the structure and evolution of planetary atmospheres both inside and outside the Solar System. The current properties of planetary atmospheres are closely related to the integrated radiation received over time and the evolutionary behavior of their host stars. In the early stages of planetary evolution, intense extreme ultraviolet (EUV) radiation from the host star can lead to the formation of a supersonic hydrodynamic regime of atmospheric outflow (planetary wind). In this case, atmospheric particles can overcome the planetary gravity, reach supersonic speed and fly away to the outer region of the Roche lobe. Predicting and estimating atmospheric loss for known exoplanets are key questions in this problem, which require the development of appropriate mathematical models suitable for interpreting observational data and creating testable new predictions. The first hydrodynamic simulations of planetary wind were based on an isothermal one-dimensional hydrodynamic model [1]. Recently, this simple, computationally inexpensive model has been applied as a tool for interpreting spectroscopic observations of various exoplanets [2–3]. The main drawback of this model is the assumption of isothermality, since in the real atmosphere the temperature has quite large variations due to heating by EUV radiation. There are also descriptions of more complex planetary wind models in the literature, for example, in the works of N. Erkaev [4–5], A. Berezutsky [6], and D. Kubyshkina [7–9], which were used to simulate runaway atmospheres of exoplanets in various stellar systems. Currently, there is increasing activity of research groups in using hydrodynamic models of planetary winds to study the long-term evolution of primary hydrogen planetary atmospheres, starting from their formation in protoplanetary clouds. For this purpose, only 1-D models have been used so far, since they require much less numerical resources compared to 2-D and especially 3-D models. However, this naturally raises the question of quantitative differences in the profiles of atmospheric parameters and the rates of atmospheric losses calculated in 1-D and 2-D models. These issues have not yet been covered in the literature. The goal of our work is to study an axially symmetric 2-D model of transonic planetary wind caused by extreme heating in the EUV range and to describe specific details of radial profiles and meridional dependences of atmospheric parameters. Special attention is also paid to issues related to the implementation of the numerical method and the choice of specific initial conditions for calculations that allow obtaining a steady-state solution with moderate computational costs.

2. Two-dimensional problem statement

Previous one-dimensional spherically symmetric formulations of the hydrodynamic escape problem from an atmosphere do not account for variations in pressure, density, and velocity of gas particles with respect to the angular deviation from the central axis directed toward the star. In reality, this spherical symmetry is broken due to the propagation and absorption of extreme ultraviolet (EUV) radiation and the increasing angular pressure gradient at larger spherical angles for a fixed distance from the planet. In this regard, spherically symmetric 1D models provide inaccurate estimates of the mass loss rate.

This study introduces a system of non-stationary hydrodynamic equations in the Euler-Entropy form, which includes neutral and ionized hydrogen atoms and describes significant entropy changes due to heating source

$$\frac{\partial \rho}{\partial t} + \frac{1}{r^2}\frac{\partial\left(\rho v_r r^2\right)}{\partial r} + \frac{1}{r}\frac{\partial(\rho v_\theta)}{\partial \theta} + \frac{\rho v_\theta \operatorname{ctg}\theta}{r} = 0, \tag{2.1}$$

$$\frac{\partial v_r}{\partial t} + v_r\frac{\partial v_r}{\partial r} + \frac{v_\theta}{r}\frac{\partial v_r}{\partial \theta} + \frac{1}{\rho}\frac{\partial P}{\partial r} = -\frac{\partial \Phi}{\partial r} + \frac{v_\theta^2}{r}, \tag{2.2}$$

$$\frac{\partial v_\theta}{\partial t} + v_r \frac{\partial v_\theta}{\partial r} + \frac{v_\theta}{r}\frac{\partial v_\theta}{\partial \theta} + \frac{1}{r\rho}\frac{\partial P}{\partial \theta} + \frac{v_\theta v_r}{r} = -\frac{1}{r}\frac{\partial \Phi}{\partial \theta}, \tag{2.3}$$

$$\frac{\partial S}{\partial t} + v_r \frac{\partial S}{\partial r} + \frac{v_\theta}{r}\frac{\partial S}{\partial \theta} = \frac{(\gamma - 1)}{P} \cdot (Q - \Lambda), \tag{2.4}$$

$$Q = \rho(1 - X)\eta\sigma_i \frac{J}{m}, \quad \Lambda = \rho^2 X(1 - X)\frac{\Lambda_0}{m^2} \exp\left(-\frac{118348}{T}\right), \tag{2.5}$$

$$\frac{\partial X}{\partial t} + v_r \frac{\partial X}{\partial r} + \frac{v_\theta}{r}\frac{\partial X}{\partial \theta} = \nu(1 - X)\frac{J}{J_\infty} - \alpha X^2 \left(\frac{\rho}{m}\right), \tag{2.6}$$

$$\cos\theta \frac{\partial J}{\partial r} - \frac{\sin\theta}{r}\frac{\partial J}{\partial \theta} = \sigma_i(1 - X)\frac{\rho_n}{m} J, \tag{2.7}$$

The system is described in spherical coordinates (r, θ), where:

- r is the radial distance from the planetary center,
- θ is the zenith angle measured from direction to the host star.

The hydrodynamic quantities are defined as:

- ρ, ρ_n: total mass density and mass density of neutral particles,
- v_r, v_θ: radial and meridional velocity components,
- P: gas pressure,
- T: gas temperature,
- γ: adiabatic index,
- $S = \ln \dfrac{P}{\rho^\gamma}$: entropy like function proportional to the physical entropy.

The ionization state and microphysics are governed by:

- m: mass of a hydrogen atom,
- X: ionization fraction (ratio of the ionized and total mass densities),
- ν, α: photoionization and recombination rates,
- σ_i: radiative photoionization cross-section,
- η: heating efficiency,
- J, J_∞: EUV radiation intensity in the upper atmosphere, EUV radiation intensity incoming from the host star far away from the planet,
- Q, Λ: radiative heating and cooling rates given in [10],
- Φ: gravitation potential given in [11].

Gas pressure consisting of partial pressures of the neutral and ionized components is given by

$$P = \rho(1 + X)k_B T/m,$$

where k_B is the Boltzmann constant.

The gravitational potential Φ incorporates three key components: planetary gravity, tidal forces from the host star, centrifugal effects from system rotation. This formulation follows the Roche lobe approximation given by N. Erkaev, H. Lammer et al. in [11].

The heating efficiency η, cross section for photoionization of hydrogen σ_i, photoionization rate ν and recombination rate α are estimated by R. Murray-Clay et al. in [10].

The equations $(2.1 - 2.4)$ represent conservation of mass, radial momentum, angular momentum, and entropy, respectively. The equations (2.6) and (2.7) describe the production of ions and the absorption of ultraviolet radiation from the host star, respectively.

The numerical solution of the governing equations yields a transonic atmospheric outflow into interplanetary space. The hydrogen envelope, heated by intense stellar irradiation, expands radially outward, eventually approaching the Roche lobe boundary [12].

The dayside mass-loss rate is determined by integrating the radial mass flux over the dayside semisphere:

$$L_{\text{day}} = \int_0^{\pi/2} L_m(\theta) \sin\theta \, d\theta, \quad \text{where} \quad L_m(\theta) = 2\pi\rho v_r(R_m, \theta)R_m^2 \tag{2.8}$$

represents the angular-dependent mass flux through a spherical surface of radius r.

The meridional mass-loss rate through the plane ($\theta = \pi/2$) representing the mass flux to the nightside of the planet is given by:

$$L_{\text{night}}(\theta) = \int_{R_s}^{R_m} L_m(r) r \, dr, \quad \text{where} \quad L_m(r) = 2\pi\rho v_\theta(r, \pi/2), \tag{2.9}$$

where R_m and R_s are the radial distances to the upper boundary of the computation domain and to the sonic point, respectively. Thus, the total mass-loss rate is

$$L_{\text{tot}} = L_{\text{day}} + L_{\text{night}}. \tag{2.10}$$

2.1. Dimensionless equations

For numerical tractability, we introduce the following dimensionless variables through characteristic normalization:

$$\tilde{P} = P/(n_0 k_B T_0), \quad \tilde{\rho} = \rho/(n_0 m), \quad \tilde{T} = T/T_0, \quad \tilde{t} = t v_{T_0}/R_{pl},$$

$$\tilde{r} = r/R_{pl}, \quad \tilde{v}_r = v_r/v_{T_0}, \quad \tilde{v}_\theta = v_\theta/(\tilde{r} v_{T_0}), \quad v_{T_0} = \sqrt{k_B T_0/m},$$

$$\tilde{\nu} = \nu R_{pl}/v_{T_0}, \quad \tilde{\alpha} = \alpha n_0 R_{pl}/v_{T_0}, \quad \tilde{J} = J/J_0, \quad \tilde{\Phi} = \Phi/v_{T_0}^2.$$

Here $n_0, \rho_0, T_0, v_{T_0}$ are the number density, mass density, effective temperature and thermal velocity at the lower boundary near the planet, where the radial distance is equal to the planet radius R_{pl}. J_0 is the EUV radiation intensity at the upper boundary of the computational domain.

The governing equations can be rewritten in dimensionless form as

$$\frac{\partial\tilde{\rho}}{\partial\tilde{t}} + \frac{1}{\tilde{r}^2}\frac{\partial\left(\tilde{\rho}\tilde{v}_r\tilde{r}^2\right)}{\partial\tilde{r}} + \frac{1}{\tilde{r}^2}\frac{\partial(\tilde{\rho}\tilde{v}_\theta)}{\partial\theta} + \frac{\tilde{\rho}\tilde{v}_\theta\cos\theta}{\tilde{r}^2} = 0,$$

$$\frac{\partial \tilde{v}_r}{\partial \tilde{t}} + \tilde{v}_r \frac{\partial \tilde{v}_r}{\partial \tilde{r}} + \frac{\tilde{v}_\theta}{\tilde{r}^2} \frac{\partial \tilde{v}_r}{\partial \theta} + \frac{1}{\tilde{\rho}} \frac{\partial \tilde{P}}{\partial \tilde{r}} = -\frac{\partial \tilde{\Phi}}{\partial \tilde{r}} + \frac{\tilde{v}_\theta^2}{\tilde{r}^3},$$

$$\frac{\partial \tilde{v}_\theta}{\partial \tilde{t}} + \tilde{v}_r \frac{\partial \tilde{v}_\theta}{\partial \tilde{r}} + \frac{\tilde{v}_\theta}{\tilde{r}^2} \frac{\partial \tilde{v}_\theta}{\partial \theta} + \frac{1}{\tilde{\rho}} \frac{\partial \tilde{P}}{\partial \theta} = -\frac{\partial \tilde{\Phi}}{\partial \theta},$$

$$\frac{\partial \tilde{S}}{\partial \tilde{t}} + \tilde{v}_r \frac{\partial \tilde{S}}{\partial \tilde{r}} + \frac{\tilde{v}_\theta}{\tilde{r}^2} \frac{\partial \tilde{S}}{\partial \theta} = \frac{(\gamma - 1)}{\tilde{P}} \cdot (\tilde{Q} - \tilde{\Lambda}),$$

$$\tilde{Q} = \tilde{Q}_0 \tilde{\rho}(1 - X)\tilde{J}, \quad \tilde{\Lambda} = \tilde{\Lambda}_0 \tilde{\rho}^2 X(1 - X) \exp\left(-\frac{b}{\tilde{T}}\right),$$

$$\frac{\partial X}{\partial \tilde{t}} + \tilde{v}_r \frac{\partial X}{\partial \tilde{r}} + \frac{\tilde{v}_\theta}{\tilde{r}^2} \frac{\partial X}{\partial \theta} = \tilde{\nu}(1 - X)\tilde{J} - \tilde{\alpha} X^2 \tilde{\rho},$$

$$\cos\theta \frac{\partial \tilde{J}}{\partial \tilde{r}} - \frac{\sin\theta}{\tilde{r}} \frac{\partial \tilde{J}}{\partial \theta} = a\tilde{\rho}\tilde{J},$$

$$a = n_0 R_{pl} \sigma_i, \quad b = \frac{118348}{T_0}, \tilde{\Lambda}_0 = \Lambda_0 \frac{n_0 R_{pl}}{m V_0^3}, \quad \tilde{Q}_0 = \eta \sigma_i J_\infty \frac{R_{pl}}{m V_0^3}.$$

2.2. Boundary and initial conditions

In this study, we adopt the system parameters of the solar-type host star TOI-421 and its warm, low-density sub-Neptune TOI-421b. The TOI-421 system was discovered in 2020, with initial system parameters reported in [13]. Subsequent refinements of these characteristics were presented in [14]. Most recently, JWST observations have enabled detailed atmospheric characterization of this exoplanet, as documented in [15]. A transmission spectrum reveals an atmosphere dominated by H/He with detectable molecular species including H_2O at near-solar abundances ($X_{H_2O} \sim 10^{-3}$ to 10^{-4}), along with tentative detections of SO_2, CO, but no evidence of CO_2 or CH_4 [15]. The resulting atmospheric composition indicates that TOI-421b has a primary atmosphere, which under the influence of intense stellar radiation experiences hydrodynamic escape.

Some planet characteristics taken from [14] are presented in Table 2.1, where $M_\oplus, R_\oplus$ are the Earth mass and radius, respectively, and M_{pl}, R_{pl} are the mass and radius of TOI-421b. T_0 is the effective temperature and J_∞ is the EUV fluxes at the distance of planet d_s. We used pressure $P_0 = 0.5$ Pa similarly as in [13].

Таблица 2.1. Планетарные характеристики TOI-421b
Table 2.1. Planetary characteristics of TOI-421b

$M_{pl}/M_\oplus$	$R_{pl}/R_\oplus$	T_0, K	orbital distance, AU	J_∞, J m^{-2} s^{-1}
6.7	2.64	922	0.0554	7452×10^{-3}

The computational domain employs a spherical coordinate system with two distinct grid configurations:

- A non-uniform radial grid with refinement toward the planetary surface:

$$\omega_{\Delta r} = \left\{ r_i = (R_m)^{\xi_i} \mid \xi_i = \frac{i}{M},\ i = \overline{1, M} \right\}.$$

- A uniform angular grid in the polar direction:

$$\omega_{\Delta \theta} = \left\{ \theta_j = \frac{(N-j)\pi}{2N} \mid j = \overline{0, N} \right\}.$$

The time stepping follows the Courant–Friedrichs–Lewy (CFL) stability criterion.

We set the lower boundary fixed at the base of the thermosphere [16–18] with the dimensionless constant values

$$\tilde{\rho}_{1,j} = 1, \quad \tilde{T}_{1,j} = 1, \quad \tilde{v}_{r_{1,j}} = \tilde{v}_{r_{2,j}}, \quad \tilde{v}_{\theta_{1,j}} = \tilde{v}_{\theta_{2,j}}, \quad \tilde{r}_1 = 1, \quad j = \overline{0, N},$$

where the first index indicates the discretization by radius, the second by angle.

The upper boundary is assumed at about $25R_{pl}$ and we set the free boundary conditions as follows

$$\tilde{\rho}_{M,j} = \tilde{\rho}_{M-1,j}, \quad \tilde{T}_{M,j} = \tilde{T}_{M-1,j}, \quad \tilde{v}_{r_{M,j}} = \tilde{v}_{r_{M-1,j}},$$
$$\tilde{v}_{\theta_{M,j}} = \tilde{v}_{\theta_{M-1,j}}, \quad \tilde{r}_M = 25, \quad j = \overline{0, N}.$$

The meridional velocity component is set to zero along the substellar line, increasing smoothly with the angular deviation from this axis. All other hydrodynamic parameters (density, temperature, radial velocity) remain unconstrained at this boundary. Similarly, free boundary conditions are imposed at the terminator.

While these conditions are well-suited for axisymmetric simulations, they may break down due to planetary orbital motion – an effect that can only be fully captured in three-dimensional models.

The initial conditions were derived from physical parameter profiles obtained in prior 1D simulations [17–18]. Additionally, the meridional velocity was initialized to zero throughout the entire computational domain. It is noteworthy that these initial conditions enable significantly faster convergence to a steady-state solution in the 2D system compared to analogous initial conditions applied to the 1D case. Furthermore, obtaining the 1D steady-state solution employs program parallelization that can be efficiently executed on conventional workstations. Consequently, the 2D steady-state solution can also be achieved within reasonable computational time without requiring high-performance supercomputing resources.

3. Numerical methods

This study employs a compact fourth-order MacCormack-type scheme combined with a fourth-order Runge-Kutta temporal integration [11–12], whose computational advantages have been demonstrated in [9–10] for 1D models. The compact MacCormack-type scheme 4/2 is used in the radial direction, and a finite-difference approximation of the first-order derivative is used in the angular direction. The key advantage of employing this compact scheme lies in its capability to perform computations at the maximum $CFL = 1.0$, ensuring both rapid convergence and numerical stability.

The computational domain utilizes a spherical grid (Fig. 3.1*a*), but to compute the radiation intensity propagating through the atmosphere along straight rays (Fig. 3.1*b*), we implement the method of characteristics with spherical grid interpolation. The geometric configuration of the characteristic rays is illustrated in Fig. 3.1*c*.

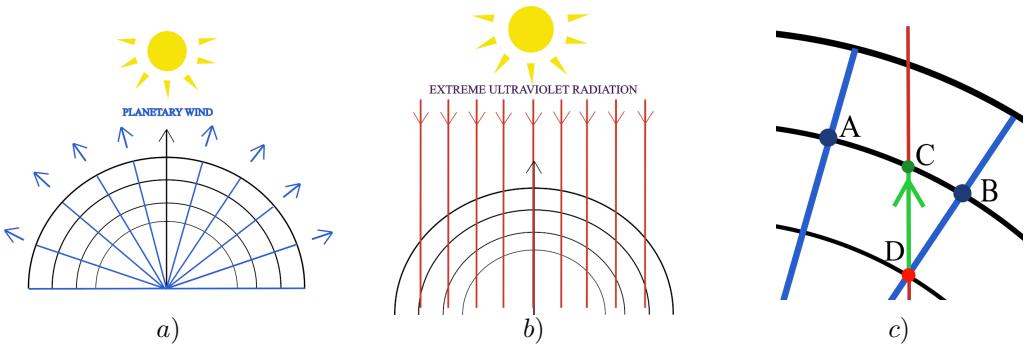

Рис. 3.1. Сетки для расчетов: *a*) расчетная сетка: сферическая геометрия области моделирования, *b*) геометрия модели: экстремальное ультрафиолетовое (EUV) излучение, проникающее в верхние слои атмосферы, *c*) расчетная сетка с характеристическими линиями: стрелка указывает характеристику, выпущенную вверх из узла “D” (зеленая)

Fig. 3.1. Grids for calculations: *a*) computational grid: spherical geometry of the simulation domain, *b*) model geometry: EUV radiation entering the upper atmosphere, *c*) computational grid with characteristic lines: the arrow indicates a characteristic emanating upward from node “D” (green)

To compute the radiation intensity values at the nodes of a spherical grid using equation 3.1, an upward characteristic is traced from each node. As illustrated in Fig. 3.1*c*, point D represents such a node on the spherical grid. The two nearest values of density and ionized particle fraction (marked as points A and B) are used to perform linear interpolation at point C. This procedure effectively transfers data from the spherical grid to a Cartesian grid to determine the radiation intensity. The interpolated value at point C is then utilized to calculate the radiation intensity at the original spherical grid node (point D). Finally, all functions on the spherical grid are updated, accounting for the two-dimensional nature of the radiation intensity.

$$\frac{\mathrm{d}J}{\mathrm{d}X} = \frac{\sigma_i \rho_0 R_{pl}}{m} \tilde{\rho} J. \tag{3.1}$$

4. Modelling results

The calculations were performed on several grids:

1. $M = 2000$, $N = 50$; 2. $M = 2000$, $N = 100$; 3. $M = 3000$, $N = 50$;
4. $M = 3000$, $N = 100$; 5. $M = 4000$, $N = 50$; 6. $M = 4000$, $N = 100$.

All plots are presented for the coarsest grid 1.
The atmosphere of a planet can be divided into several layers (Figure 4.1):

- Lower atmosphere $r = 1 - 1.8R_{pl}$;
- Photosphere $r > 2.15R_{pl}$;
- Superdonic region $r > 1.8R_{pl}$, where flow becomes supersonic and hydrodynamic wind forms;
- Roche lobe boundary $r \approx 10R_{pl}$;
- Exobase $r > 25R_{pl}$, where the average free path of a molecule $\lambda(z_{ex})$ becomes comparable to the altitude scale $H(z_{ex})$.

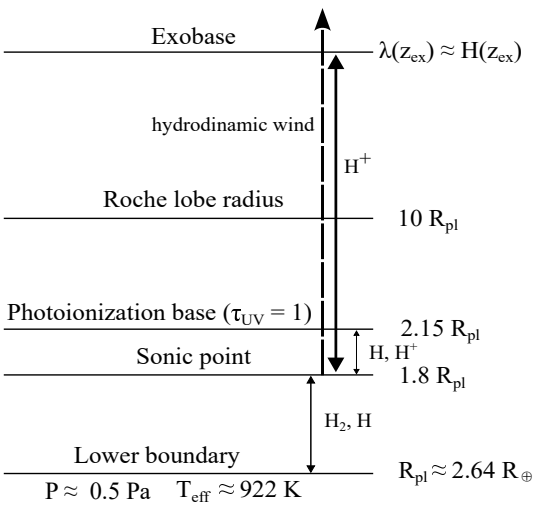

Рис. 4.1. Для планеты TOI-421b поверхность с оптической глубиной $\tau = 1$ расположена на $r \approx 2.15R_{pl}$. Звуковая точка находится на отметке $r \approx 1.8R_{pl}$, и выше этой точки формируется гидродинамический ветер. Граница полости Роша — $r \approx 10R_{pl}$

Fig. 4.1. For a planet TOI-421b the surface with optical depth $\tau = 1$ is located $r \approx 2.15R_{pl}$. The sonic point lies at $r \approx 1.8R_{pl}$ and above this point the hydrodinamic wind forms. The Roche lobe boundary is at $r \approx 10R_{pl}$

The results of our numerical simulations demonstrate the variations of atmospheric parameters depending on the radial distance and angle in the case of supersonic outflow. For example, Figure 4.2 shows the atmospheric heating rate in dependence on the radial distance and zenith angle. The atmospheric heating rate peaks at the substellar line and then decreases with increasing angle θ. This occurs because the maximum EUV radiation intensity is observed at the substellar line, where it reached maximum at approximately $\tilde{r} \approx 1.3R_{pl}$ (Fig. 4.2*b*). At a fixed radial distance, the heating rate decreases significantly with increasing angle θ (Fig. 4.2*a*). This occurs because the maximum EUV radiation intensity is observed at the substellar line. In this region, the accumulated energy from stellar radiation raises the gas temperature to its peak value, as seen in Figure 4.3*a*. Note that the normalized temperature exhibits minimal variation with zenith angle, indicating weak dependence on incident star flux for temperature. The atmosphere heats up through absorption of EUV radiation, expands, and increases its population of ionized hydrogen atoms before eventually

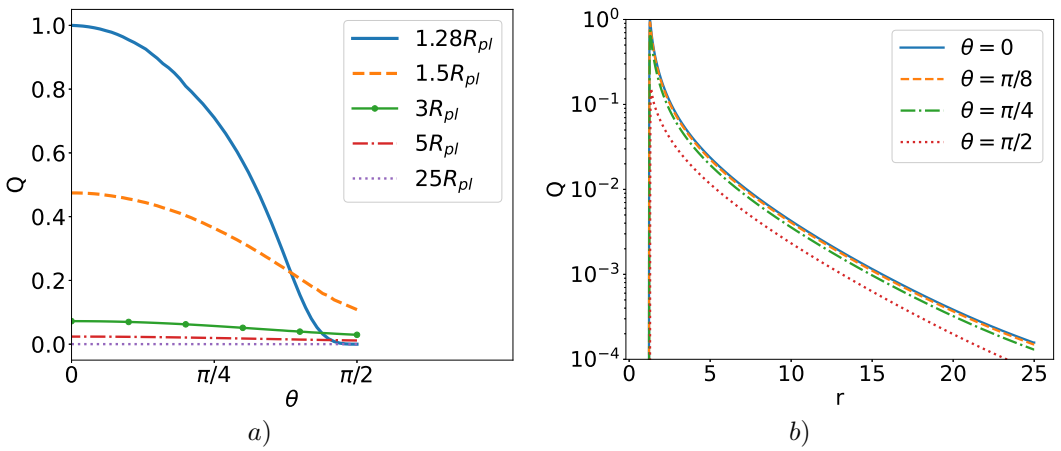

Рис. 4.2. Зависимость в логарифмическом масштабе нормализованной объемной скорости нагрева от: *a*) зенитного угла, *b*) радиального расстояния. Скорость нагрева учитывает поглощение атмосферой звездного излучения и нормализована относительно ее максимального значения

Fig. 4.2. Dependence on a logarithmic scale of the normalized volumetric heating rate on: *a*) zenith angle, *b*) radial distanse. The heating rate accounts for atmospheric absorption of star radiation and is normalized to its maximum value

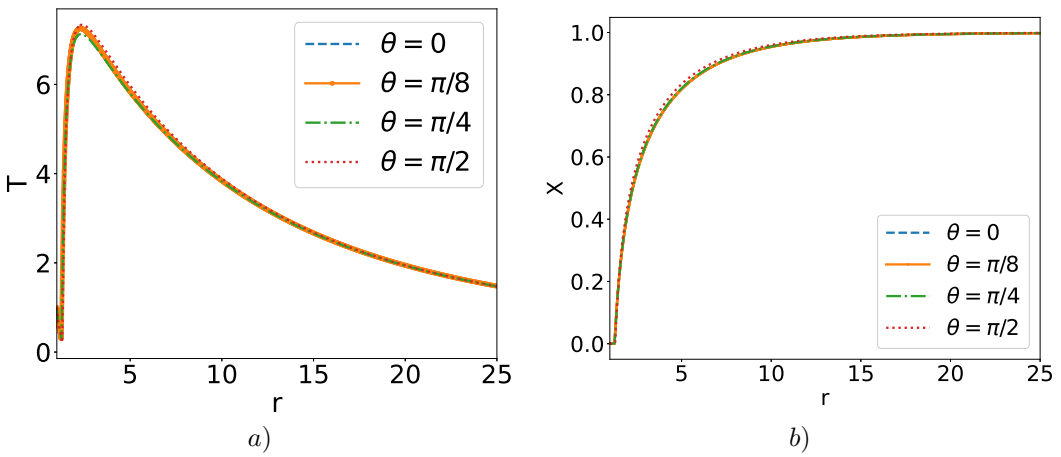

Рис. 4.3. *a*) Нормированная температура в зависимости от радиального расстояния, *b*) доля ионизированных частиц в зависимости от радиального расстояния

Fig. 4.3. *a*) Dependence of normalized temperature on radial distanse, *b*) the fraction of ionized particles as a function of radial distance

cooling down. As seen in Figure 4.3*b*, the 50% ionization threshold is reached at a distance of $r \approx 2.28R_{pl}$, marking the transition to a predominantly ionized atmospheric layer.

Figure 4.4*a* presents the atmospheric pressure as function of the radial distance. The pressure first decreases exponentially in the subsonic region near the planet's boundary, and

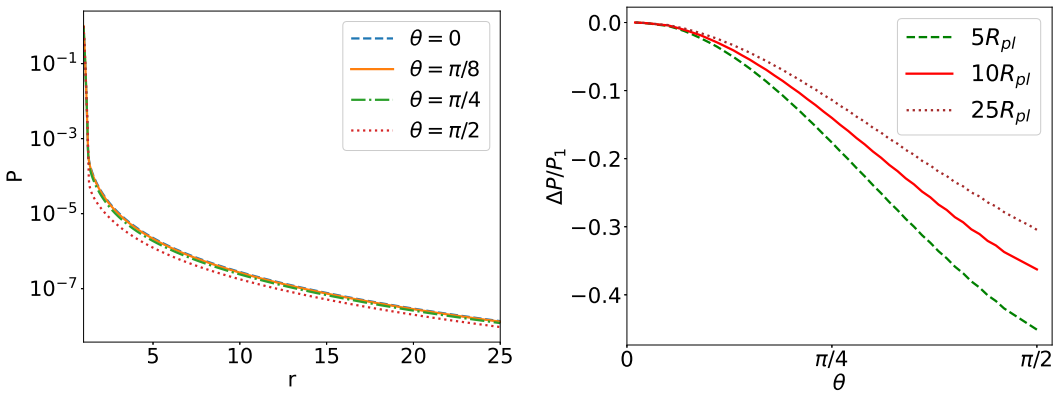

Рис. 4.4. *a*) Нормализованное давление как функция радиального расстояния для различных зенитных углов, *b*) изменение давления, отнесенного к его значению на оси симметрии P_1, относительно угла на трех радиальных расстояниях

Fig. 4.4. *a*) The normalized pressure as function of the radial distance for different zenith angles, *b*) variation of the pressure normalized to its substellar value P_1 with respect to the angle at three radial distances

then its behavior becomes much flatter in the supersonic region. Also Figure 4.4*b* shows the relative change of the pressure with respect to zenith angle. Here $\Delta P = P - P_1$, where P_1 corresponds to the substellar axis at the same radial distance. The pressure gradient creates meridional flows, and, consequently, the meridional velocity increases with the deviation angle from the substellar point, as illustrated in Figures 4.5.

The Figure 4.6*a* shows the radial velocity v_r as function of the radial distance for different zenith angles. The velocity profiles corresponding to various angles are rather close to each other. The dimensional maximum velocity reached at upper boundary is 33 km/s.

The total dimensionless mass loss rate on the dayside was computed using Eq. (2.8), with its zenith-angle distribution shown in Figure 4.5*b*. The dimensional mass loss rates are:

- Dayside: $L_{day} \approx 1.0 \cdot 10^7\,\mathrm{kg\,s^{-1}}$ (Eq. (2.8));
- Nightside: $L_{night} \approx 0.449 \cdot 10^7\,\mathrm{kg\,s^{-1}}$ (Eq. (2.9));
- Total: $L_{tot} \approx 1.449 \cdot 10^7\,\mathrm{kg\,s^{-1}}$ (Eq. (2.10)).

Comparison of the mass flow rates obtained using grid 1 ($M = 2000, N = 50$) and the finest grid 6 ($M = 4000, N = 100$) shows that the mass flow rate on the dayside differs by 2%, while the total mass flow rate differs by approximately 1%. At the same time, the computation time on the finest grid is more than twice that on the coarsest grid. This leads to the conclusion that it is reasonable to use less detailed grids to obtain qualitatively accurate results faster.

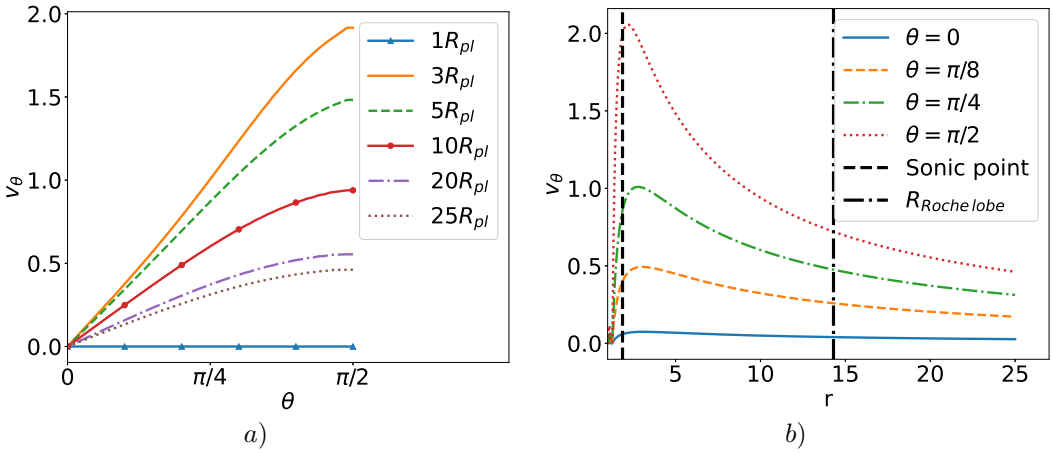

Рис. 4.5. *a*) Зависимость меридиональной скорости от зенитного угла, *b*) зависимость меридиональной скорости от радиального расстояния с обозначением точки, звуковой скорости (левая вертикальная линия) и границы полости Роша (правая вертикальная линия)

Fig. 4.5. *a*) Dependence of the meridional velocity on the zenith angle, *b*) dependence of the meridional velocity on the radial distance with the designation of the point corresponding to the speed of sound (left vertical line) and the boundary of the Roche lobe (right vertical line)

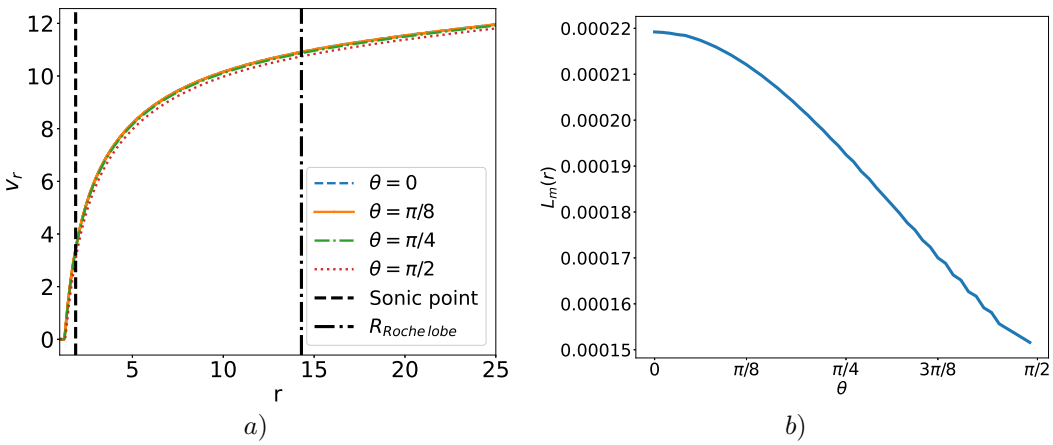

Рис. 4.6. *a*) Профиль радиальной скорости в зависимости от радиального расстояния. Вертикальные линии обозначают точки скорости звука и границы полости Роша, *b*) распределение потока массы в безразмерных единицах по зенитному углу

Fig. 4.6. *a*) Radial velocity profile as a function of radial distance. Vertical lines mark sonic point and the Roche lobe boundary, *b*) distribution of mass flux in dimensionless units by zenith angle

5. Summary

Our study concerns two-dimensional formulation of the problem of outflow of a planet's atmosphere, which is caused by absorption of extreme ultraviolet radiation incoming from

the host star. A system of hydrodynamic equations in the Euler form was used in combination with the entropy production equation, which describes in detail the thermodynamics of the atmospheric gas. A stationary solution in spherical coordinates was obtained by the time relaxation method using an explicit 4-step in time numerical scheme of the MacCormack type with a compact approximation of derivatives with respect to the radius, which provides stability at the Courant-Friedrichs-Lewy number equal to 1. A sufficiently rapid establishment of the stationary outflow regime is reached by setting as initial state the spherically symmetric distribution of density, radial velocity and temperature, previously found from the one-dimensional model. A recently discovered exoplanet TOI-421b was chosen as a particular object of application of our model, for which two-dimensional features of the atmospheric outflow were analyzed. It is shown that the temperature, radial velocity, pressure and density of the atmospheric gas are monotonically decreasing functions of the zenith angle for a fixed radial distance. In this case, the angular dependence is most strongly pronounced for the density and pressure. The meridional component of the velocity increases monotonically with increasing zenith angle and provides the entrainment of atmospheric gas to the night side. In this case, the total mass flow to the day and night sides is about $1.449 \cdot 10^7\,\mathrm{kg\,s^{-1}}$.

Acknowledgements. This work is supported by the Krasnoyarsk Mathematical Center and financed by the Ministry of Science and Higher Education of the Russian Federation in the framework of the establishment and development of regional Centers for Mathematics Research and Education (Agreement No. 075-02-2025-1606).

References

1. E. N. Parke, "Dynamics of the interplanetary gas and magnetic fields", *Astrophysical Journal*, **128** (1958), 664 p. DOI: 10.1086/146097

2. L. A. Dos Santos, A. A. Vidotto, Shreyas Vissapragada, M. K. Alam, R. Allart, V. Bourrier, J. Kirk, J. V. Seidel, D. Ehrenreich, "p-winds: An open-source Python code to model planetary outflows and upper atmospheres", *Astronomy & Astrophysics*, **659**:A62 (2022). DOI: 10.1051/0004-6361/202142038

3. P. McCreery, L. A. Dos Santos, N. Espinoza, R. Allart, J. Kirk, "Tracing the Winds: A Uniform Interpretation of Helium Escape in Exoplanets from Archival Spectroscopic Observations", *The Astrophysical Journal*, **980** (2025), 125. DOI: 10.3847/1538-4357/ada6b9

4. N. V. Erkaev, H. Lammer, P. Odert, K. G. Kislyakova, C. P. Johnstone, M. Güdel, M. L. Khodachenko, "EUV-driven mass-loss of protoplanetary cores with hydrogen-dominated atmospheres: the influences of ionization and orbital distance", *Monthly Notices of the Royal Astronomical Society*, **460**:2 (2016), 1300–1309. DOI: 10.1093/mnras/stw935

5. N. V. Erkaev, M. Scherf, O. Herbort, H. Lammer, P. Odert, D. Kubyshkina, M. Leitzinger, P. Woitke, C. O'Neill, "Modification of the radioactive heat budget of Earth-like exoplanets by the loss of primordial atmospheres", *Monthly Notices of the Royal Astronomical Society*, **518**:3 (2023), 3703–3721. DOI: 10.1093/mnras/stac3168

6. A. G. Berezutsky, I. F. Shaikhislamov, M. S. Rumenskikh, M. L. Khodachenko, H. Lammer, I. B. Miroshnichenko, "On the transit spectroscopy features of warm Neptunes in the TOI-421 system, revealed with their 3D aeronomy simulations", *Monthly Notices of the Royal Astronomical Society*, **515**:1 (2022), 706–715. DOI: 10.1093/mnras/stac1633

7. D. Kubyshkina, A. A. Vidotto, "How does the mass and activity history of the host star affect the population of low-mass planets?", *Monthly Notices of the Royal Astronomical Society*, **50**:2 (2021), 2034–2050. DOI: 10.1093/mnras/stab897

8. D. Kubyshkina, A. A. Vidotto, C. Villarreal D'Angelo, S. Carolan, G. Hazra, I. Carleo, "Atmospheric mass-loss and stellar wind effects in young and old systems – I. Comparative 3D study of TOI-942 and TOI-421 systems", *Monthly Notices of the Royal Astronomical Society*, **510**:2 (2022), 2111–2126. DOI: 10.1093/mnras/stab3594

9. D. Kubyshkina, A. A. Vidotto, C. Villarreal D'Angelo, S. Carolan, G. Hazra, I. Carleo, "Atmospheric mass loss and stellar wind effects in young and old systems – II. Is TOI-942 the past of TOI-421 system?", *Monthly Notices of the Royal Astronomical Society*, **510**:2 (2022), 3039–3045. DOI: 10.1093/mnras/stab3620

10. R. A. Murray-Clay, E. I. Chiang, N. Murray, "Atmospheric escape from hot Jupiters", *The Astrophysical Journal*, **693** (2009), 23–42. DOI: 10.1088/0004-637X/693/1/23

11. N. V. Erkaev, Yu. N. Kulikov, H. Lammer, F. Selsis, D. Langmayr, G. F. Jaritz, H. K. Biernat, "Roche lobe effects on the atmospheric loss from "Hot Jupiters"", *Astronomy & Astrophysics*, **472**:1 (2007), 329–334. DOI: 10.1051/0004-6361:20066929

12. A. Vidal-Madjar, A. Lecavelier des Etangs, ""Osiris"(HD209458b), an Evaporating Planet", *Extrasolar Planets: Today and Tomorrow, ASP Conference Proceedings.* Vol. 321 (Institut D'Astrophysique de Paris, France), 2004, 152–160, arXiv: https://arxiv.org/abs/astro-ph/0312382.

13. I. Carleo, D. Gandolfi, O. Barragán, *et al.*, "The multiplanet system TOI-421: A warm Neptune and a super puffy Mini-Neptune transiting a G9 V star in a visual binary", *The Astronomical Journal*, **160**:3 (2020), 23 p. DOI: 10.3847/1538-3881/aba124

14. A. F. Krenn, D. Kubyshkina, L. Fossati, *et al.*, "Characterisation of the TOI-421 planetary system using CHEOPS, TESS, and archival radial velocity data", *Astronomy & Astrophysics*, **686**:A301 (2024), 20 p. DOI: 10.1051/0004-6361/202348584

15. B. Davenport, E. M.-R. Kempton, M. C. Nixon, *et al.*, "TOI-421 b: A Hot Sub-Neptune with a Haze-free, Low Mean Molecular Weight Atmosphere", *The Astrophysical Journal Letters*, **984**:L44 (2025), 12 p. DOI: 10.3847/2041-8213/adcd76

16. N. V. Erkaev, H. Lammer, *et al.*, "XUV exposed non-hydrostatic hydrogen-rich upper atmospheres of terrestrial planets. Part I: Atmospheric expansion and thermal escape", *Astrobiology Journal*, **13** (2013), 1011–1029. DOI: 10.1089/ast.2012.0957

17. N. V. Erkaev, K. D. Gorbunova, "Hydrodynamic models of outflow of the planetary atmospheres", *Computational technologies*, **29**:1 (2024), 5–17 (In Russ). DOI: 10.25743/ICT.2024.29.1.002

18. N. V. Erkaev, K. D. Gorbunova, "Magnetic Barrier in Front of Exoplanets Interacting with Stellar Wind", *Problems of Geocosmos–2022*. Vol. ICS 2022, Springer Proceedings in Earth and Environmental Sciences, eds. A. Kosterov, E. Lyskova, I. Mironova, S. Apatenkov, S. Baranov, Springer, Cham, 2023, 251–265 DOI: 10.1007/978-3-031-40728-4_18.

19. R. Hixon, E. Turkel, "Compact Implicit MacCormack-Type Schemes with High Accuracy", *Journal of Computational Physics*, **158** (2000), 51–70. DOI: 10.1006/jcph.1999.6406

20. K. D. Gorbunova, N. V. Erkaev, "Compact MacCormack-type Schemes Applied for Atmospheric Escape Problem", *Journal of Siberian Federal University. Mathematics & Physics*, **15**:4 (2022), 500–509. DOI: 10.17516/1997-1397-2022-15-4-500-509

Submitted 05.06.2025; Revised 06.10.2025; Accepted

The authors have read and approved the final manuscript.
Conflict of interest: The authors declare no conflict of interest.

Список литературы

1. Parker E. N. Dynamics of the interplanetary gas and magnetic fields. *Astrophysical Journal*. 1958. Vol. 128. P. 664. DOI: 10.1086/146097

2. Dos Santos L. A., Vidotto A. A., Vissapragada S., Alam M. K., Allart R., Bourrier V., Kirk J., Seidel J. V., Ehrenreich D. p-winds: An open-source Python code to model planetary outflows and upper atmospheres. *Astronomy & Astrophysics*. 2022. Vol. 659, no. A62. DOI: 10.1051/0004-6361/202142038

3. McCreery P., Dos Santos L. A., Espinoza N., Allart R., Kirk J. Tracing the Winds: A Uniform Interpretation of Helium Escape in Exoplanets from Archival Spectroscopic Observations. *The Astrophysical Journal*. 2025. Vol. 980. P. 125. DOI: 10.3847/1538-4357/ada6b9

4. Erkaev N. V., Lammer H., Odert P., Kislyakova K.G., Johnstone C. P., Güdel M., Khodachenko M. L. EUV-driven mass-loss of protoplanetary cores with hydrogen-dominated atmospheres: the influences of ionization and orbital distance. *Monthly Notices of the Royal Astronomical Society*. 2016. Vol. 460, no. 2. P. 1300–1309. DOI: 10.1093/mnras/stw935

5. Erkaev N. V., Scherf M., Herbort O., Lammer H., Odert P., Kubyshkina D., Leitzinger M., Woitke P., O'Neill C. Modification of the radioactive heat budget of Earth-like exoplanets by the loss of primordial atmospheres. *Monthly Notices of the Royal Astronomical Society*. 2023. Vol. 518, no. 3, P. 3703–3721. DOI: 10.1093/mnras/stac3168

6. Berezutsky A. G., Shaikhislamov I. F., Rumenskikh M. S., Khodachenko M. L., Lammer H., Miroshnichenko I.Ḃ. On the transit spectroscopy features of warm Neptunes in the TOI-421 system, revealed with their 3D aeronomy simulations. *Monthly Notices of the Royal Astronomical Society*. 2022. Vol. 515, no. 1. P. 706–715. DOI: 10.1093/mnras/stac1633

7. Kubyshkina D., Vidotto A. A. How does the mass and activity history of the host star affect the population of low-mass planets? *Monthly Notices of the Royal Astronomical Society*. 2021. Vol. 50, no. 2. P. 2034–2050. DOI: 10.1093/mnras/stab897

8. Kubyshkina D., Vidotto A. A., Villarreal D'Angelo C., Carolan S., Hazra G., Carleo I. Atmospheric mass-loss and stellar wind effects in young and old systems – I. Comparative 3D study of TOI-942 and TOI-421 systems. *Monthly Notices of the Royal Astronomical Society*. 2022. Vol. 510, no. 2. P. 2111–2126. DOI: 10.1093/mnras/stab3594

9. Kubyshkina D., Vidotto A. A., Villarreal D'Angelo C., Carolan S., Hazra G., Carleo I. Atmospheric mass loss and stellar wind effects in young and old systems – II. Is TOI-942 the past of TOI-421 system? *Monthly Notices of the Royal Astronomical Society*. 2022. Vol. 510, no. 2. P. 3039–3045. DOI: 10.1093/mnras/stab3620

10. Murray-Clay R. A., Chiang E. I., Murray N. Atmospheric escape from hot Jupiters. *The Astrophysical Journal*. 2009. Vol. 693. P. 23–42 DOI: 10.1088/0004-637X/693/1/23

11. Erkaev N. V., Kulikov Yu. N., Lammer H., et al. Roche lobe effects on the atmospheric loss from "Hot Jupiters". *Astronomy & Astrophysics*. 2007. Vol. 472, no. 1. P. 329–334. DOI: 10.1051/0004-6361:20066929

12. Vidal-Madjar A., Lecavelier des Etangs A. "Osiris" (HD209458b), an evaporating planet. *Extrasolar Planets: Today and Tomorrow, ASP Conference Proceedings*. 2004. Vol. 321. P. 152–160. DOI: 10.48550/arXiv.astro-ph/0312382

13. Carleo I., Gandolfi D., Barragán O. The multiplanet system TOI-421: A warm Neptune and a super puffy Mini-Neptune transiting a G9 V star in a visual binary. *The Astronomical Journal*. 2020. Vol. 160. P. 114–137. DOI: 10.3847/1538-3881/aba124

14. Krenn A. F., Kubyshkina D., Fossati L. Characterisation of the TOI-421 planetary system using CHEOPS, TESS, and archival radial velocity data. *Astronomy & Astrophysics*. 2024. Vol. 686, no. A301, 20 p. DOI: 10.1051/0004-6361/202348584

15. Davenport B., Kempton E. M.-R., Nixon M. C. TOI-421 b: A Hot Sub-Neptune with a Haze-free, Low Mean Molecular Weight Atmosphere. *The Astrophysical Journal Letters*. 2025. Vol. 984, no. L44. 12 p. DOI: 10.3847/2041-8213/adcd76

16. Erkaev N. V., Lammer H. XUV exposed non-hydrostatic hydrogen-rich upper atmospheres of terrestrial planets. Part I: Atmospheric expansion and thermal escape. *Astrobiology Journal*. 2013. Vol. 13. P. 1011–1029. DOI: 10.1089/ast.2012.0957

17. Еркаев Н. В., Горбунова К. Д. Компактная разностная схема для гидродинамической модели истечения атмосфер планет // *Вычислительные технологии*. 2024. Т. 29, № 1. С. 5–17. DOI: 10.25743/ICT.2024.29.1.002

18. Erkaev N. V., Gorbunova K. D. Magnetic Barrier in Front of Exoplanets Interacting with Stellar Wind. *Problems of Geocosmos–2022. Springer Proceedings in Earth and Environmental Sciences*. Cham: Springer, 2023. Vol. ICS 2022. P. 251–265. DOI: 10.1007/978-3-031-40728-4_18

19. Hixon R., Turkel E. Compact Implicit MacCormack-Type Schemes with High Accuracy. *Journal of Computational Physics*. 2000. Vol. 158. P. 51–70. DOI: 10.1006/jcph.1999.6406

20. Gorbunova K. D., Erkaev N. V. Compact MacCormack-type Schemes Applied for Atmospheric Escape Problem. *Journal of Siberian Federal University. Mathematics & Physics*. 2022. Vol. 15, no. 4. P. 500–509. DOI: 10.17516/1997-1397-2022-15-4-500-509

Поступила 05.06.2025; доработана после рецензирования 06.10.2025; принята к публикации

Авторы прочитали и одобрили окончательный вариант рукописи.
Конфликт интересов: авторы заявляют об отсутствии конфликта интересов.